

Hydroelastic vibration analysis of liquid-contained rectangular tanks

Kyeong-Hoon Jeong*

SMART Development Department, Korea Atomic Energy Research Institute,
1045 Daedeokdaero, Yuseong, Daejeon 305-353, Korea

(Received February 6, 2011, Revised August 9, 2011, Accepted October 12, 2011)

Abstract. This paper presents a theoretical analysis for the free vibration of rectangular tanks partially filled with an ideal liquid. Wet dynamic displacements of the tanks are approximated by combining the orthogonal polynomials satisfying the boundary conditions, since the rectangular tanks are composed of four rectangular plates. The classical boundary conditions of the tanks at the top and bottom ends are considered, such as clamped, simply supported, and clamped-free boundary conditions. As the facing rectangular plates are assumed to be geometrically and structurally identical, the vibration modes of the facing plates of the tanks can be divided into two categories: symmetric and antisymmetric modes with respect to the planes passing through the center of the tanks and perpendicular to the free liquid surface. The liquid displacement potentials satisfying the Laplace equation and liquid boundary conditions are derived, and the wet dynamic modal functions of a quarter of the tanks can be expanded by the finite Fourier transform for compatibility requirements along the contacting surfaces between the tanks and liquid. An eigenvalue problem is derived using the Rayleigh-Ritz method. Consequently, the wet natural frequencies of the rectangular tanks can be extracted. The proposed analytical method is verified by observing an excellent agreement with three-dimensional finite element analysis results. The effects of the liquid level and boundary condition at the top and bottom edges are investigated.

Keywords: hydroelastic vibration; rectangular tanks; liquid-coupled vibration; Rayleigh-Ritz method; orthogonal polynomials; Gram-Schmidt process

1. Introduction

Rectangular tanks have been used for liquid storage in many engineering fields. For instance, a rectangular spent fuel storage tank filled with cooling water should meet the most stringent safety requirements. It should be designed to withstand a wide variety of external impacts such as earthquakes. The fresh water storage tank in bulk carriers is a rectangular steel shell structure and the water level of the tank will gradually decrease during voyage. As the dynamic characteristic of the water storage tank is changed, the response due to the external loading such as vibratory loadings from engines and sea waves will also change. Hence the dynamic characteristics of liquid-filled rectangular tanks are of considerable practical interest.

Many investigators (Cheung and Zhou 2000, Ergin and Uğurlu 2003, Hashemi *et al.* 2010, Kerboua *et*

*Corresponding author, Ph.D., E-mail: khjeong@kaeri.re.kr

al. 2008, Liang *et al.* 2001, Uğurlu *et al.* 2008, Yadykin *et al.* 2003, Zhou and Cheung 2000) have developed some approximate solutions to predict the changes in the natural frequencies when a rectangular plate is in contact with a liquid. Also, an analytical method to calculate the natural frequencies of two identical rectangular plates coupled with a bounded fluid was suggested (Jeong *et al.* 2003, Jeong and Kim 2009). However, to date, there has been minimal research regarding a flexible rectangular tank filled with a liquid. Zhou and Liu (2007) developed a theory on the three-dimensional dynamic characteristics of flexible rectangular tanks partially filled with liquid using a combination of the Rayleigh-Ritz method. The admissible functions in the reference were selected as a beam function with an internal point support, and the free surface boundary condition is suggested at the center of the liquid-filled tank for the antisymmetric modes. However, this seems to be an inappropriate assumption.

This paper will present a theory to calculate the wet natural frequencies of rectangular tanks with several classical boundary conditions, partially filled with an ideal liquid, using the Rayleigh-Ritz method and finite Fourier transform based on the orthogonal polynomial functions and appropriate displacement potential function of the liquid. The proposed method will be verified by performing three-dimensional finite element analyses. The effect of the liquid depth on the natural frequencies will be discussed. In the finite element analysis, as the liquid depth of the tanks increases, the number of liquid elements increase drastically. Hence, an increase of the liquid depth requires much calculation time in the finite element analysis. However, the proposed theoretical method can reduce the computation time to calculate the wet natural frequencies of the liquid-filled rectangular tanks regardless of the liquid depth.

2. The Rayleigh-Ritz approach

2.1 Dynamic displacement of rectangular tanks

A liquid-filled rectangular tank has a height of a , length of b , width of c , and thickness of h as depicted in Fig. 1. The ideal liquid of the depth, d , is partially contained in the tank. Since the liquid storage tank is composed of four rectangular plates, the vibration modes of the tank can be classified into two types of modes, according to the relative displacement between the plates facing each other: that is, out-of-phase and in-phase modes. From another point of view, the vibration modes can be categorized into four types of modes according to whether the deformed shapes are symmetric or antisymmetric with respect to the planes passing through the center of the tank. That is to say, S-S (Symmetric-Symmetric) modes, S-A (Symmetric-Antisymmetric) modes, A-S (Antisymmetric-Symmetric) modes, and A-A (Antisymmetric-Antisymmetric) modes as illustrated in Fig. 2. The symmetric modes indicate a reflection symmetric pattern; on the contrary, antisymmetric modes show a rotation symmetric configuration. The S-S modes are symmetric with respect to the x - and y -axes, simultaneously, the S-A modes are symmetric with respect to the y -axis and antisymmetric with respect to the x -axis, the A-S modes are antisymmetric with respect to the y -axis and symmetric with respect to the x -axis, and the A-A modes are all antisymmetric with respect to the x - and y - axes.

Therefore, the whole liquid-contained tank can be analyzed by taking into account a quarter of the liquid-contacting rectangular tank, as shown in Fig. 3. The two semi-plates of the quarter can be regarded as a line-supported rectangular plate by introducing a new coordinate system, namely a ξ - z

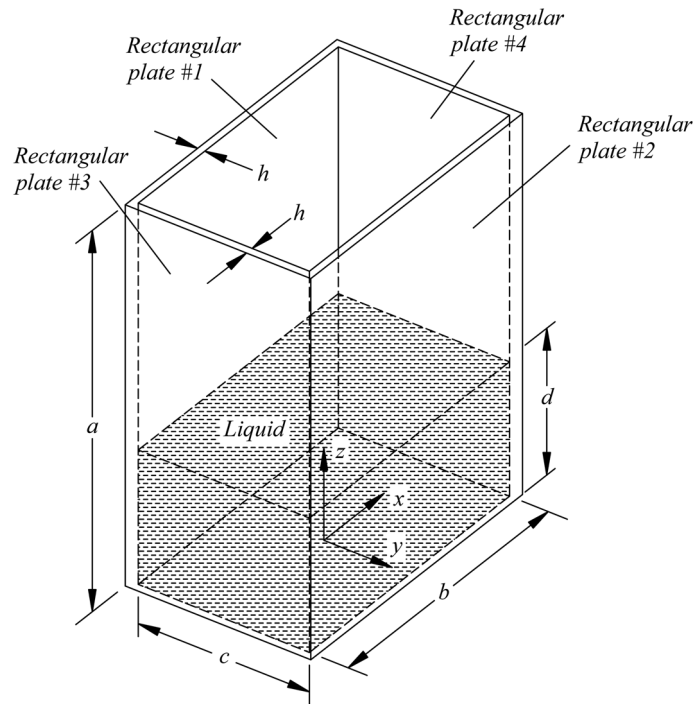


Fig. 1 A rectangular tank partially filled with a liquid

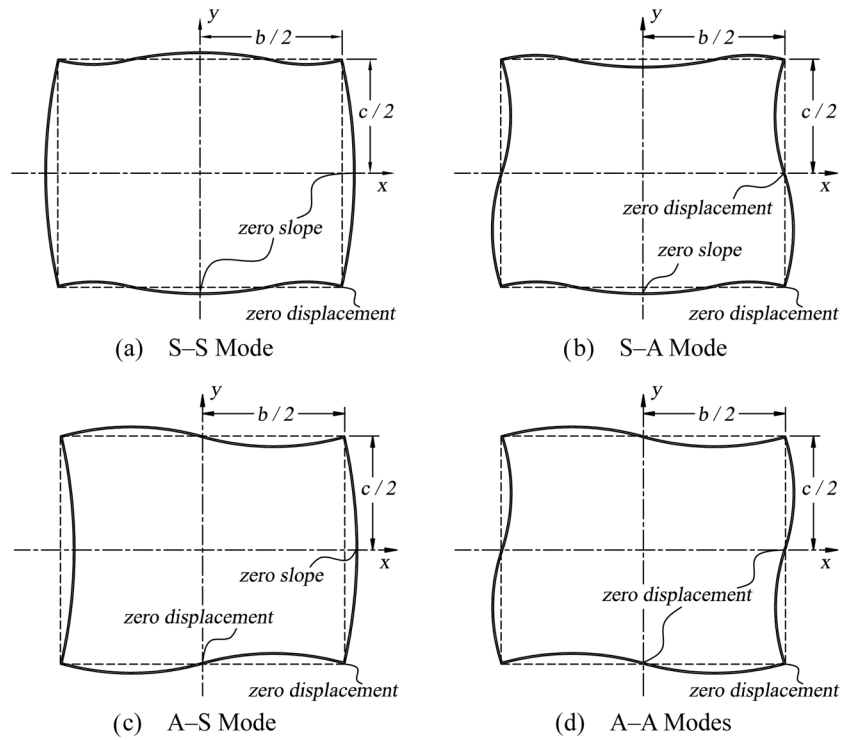


Fig. 2 Mode category of a rectangular tank partially filled with a liquid

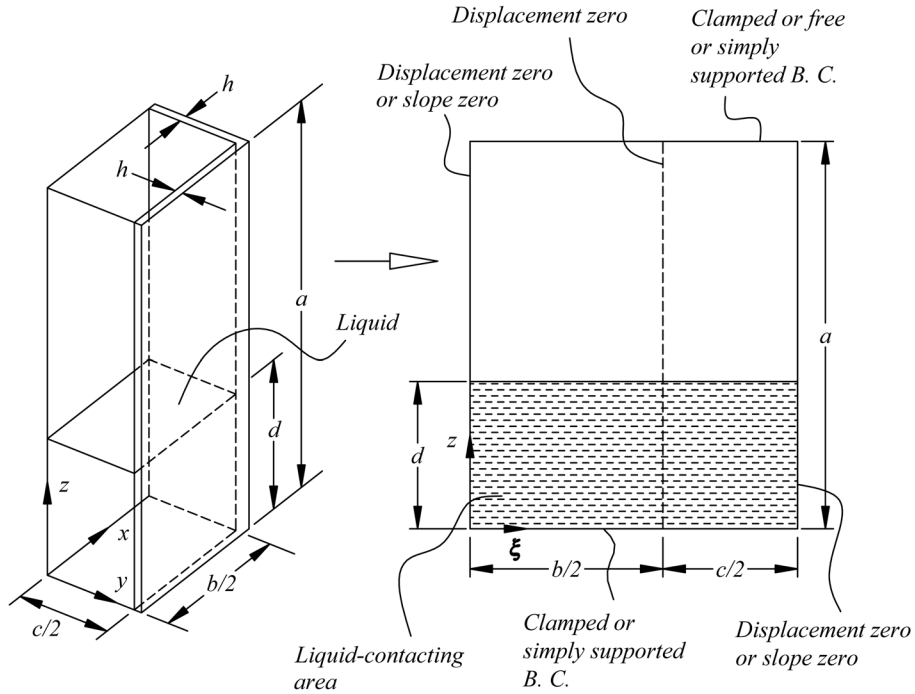


Fig. 3 Theoretical model of a rectangular tank partially filled with a liquid

plane. Each mode shape of the plate in the ξ - z plane can be approximated by a combination of a finite number of admissible functions, $W_{mn}(\xi, z)$, and the corresponding unknown coefficients, q_{mn}

$$w(\xi, z, t) = \sum_{m=1}^M \sum_{n=1}^N q_{mn} W_{mn}(\xi, z) \exp(i\omega t) \tag{1}$$

where $i = \sqrt{-1}$ and ω is the circular natural frequency of the dry or wet tanks. It is essential to select a set of admissible functions to describe the vibratory motion of the rectangular tanks. Generally, the sinusoidal and hyperbolic functions have been used as the admissible functions for the dynamic analysis of clamped rectangular plates. However, note that the required precision of the mode shape parameters drastically increases as the number of modes increases. Additionally, as the admissible functions, the sinusoidal functions are not compatible with the liquid motion when a tank is simply supported at the top and bottom edges. That is to say, the sine functions to describe transverse displacements of the simply supported rectangular tank in the vertical direction are not compatible with the cosine functions to present the liquid motion written by the first derivative of the displacement potential function. Therefore, a set of orthogonal polynomial functions is introduced as the admissible functions. The indices m and n in Eq. (1) indicate the m -th order polynomial in the ξ -direction and the n -th order polynomial in the z -direction, respectively. The transverse modal function can be defined by a multiplication of the ξ - and z -directional admissible functions, $H_m(\xi)$ and $F_n(z)$

$$W_{mn}(\xi, z) = H_m(\xi)F_n(z) \tag{2}$$

The admissible functions, $H_m(\xi)$ and $F_n(z)$ are assumed to be a set of orthogonal polynomials

satisfying the geometric and natural boundary conditions.

$$H_m(\xi) = \sum_{k=0}^Q A_{mk} \left(\frac{2\xi}{b+c} \right)^k = \sum_{k=0}^Q A_{mk} \zeta^k \tag{3}$$

$$F_n(z) = \sum_{j=0}^P B_{nj} \left(\frac{z}{a} \right)^j = \sum_{j=0}^P B_{nj} \eta^j \tag{4}$$

where the frequency parameters A_{mk} and B_{nj} are the coefficients determined by the boundary condition and the normalization of the admissible functions. The non-dimensional variables are defined as $2\xi/(b+c) = \zeta$ and $z/a = \eta$. The numbers of expanding terms k and j indicate the exponents of the polynomials. Since the admissible functions are orthogonal with respect to the others, and the coefficients A_{mk} and B_{nj} are normalized with respect to the length of $(b+c)/2$ and a , respectively, Eqs. (5) and (6) can be obtained.

$$\int_0^{(b+c)/2} H_m(\xi) H_u(\xi) d\xi = \begin{cases} 0 & \text{if } m \neq u \\ \frac{b+c}{2} & \text{if } m = u \end{cases} \tag{5}$$

$$\int_0^a F_n(z) F_v(z) dz = \begin{cases} 0 & \text{if } n \neq v \\ a & \text{if } n = v \end{cases} \tag{6}$$

where, similarly, the indices u and v also indicate the u -th polynomial in the ξ -direction, and the v -th polynomial in the z -direction, respectively.

2.2 Determination of orthogonal admissible functions

The first admissible functions can be obtained from the boundary conditions of the L -shape plates in the cross section. The orthogonal polynomials in the interval $[0, (b+c)/2]$ will be classified into the four categories according to the relative mode shapes. Moreover, the selected plate in the transformed coordinates ξ - z is assumed to be line-supported along $\xi = b/2$ in order to idealize the corners of the rectangular tanks, regardless of the category. So

$$H_m(\xi)|_{\xi=b/2} = 0 \tag{7}$$

Obviously, no restriction is applied along the corners except the displacement constraint of Eq. (7). Hence, the slope along the corners need not be zero. In addition, it would be interesting to observe the symmetry in the dynamic deformation of the dry or wet system. The boundary conditions of the folded L -shape plate to simulate a quarter of the tank will be written for S-S modes

$$\left. \frac{dH_m(\xi)}{d\xi} \right|_{\xi=0} = \left. \frac{dH_m(\xi)}{d\xi} \right|_{\xi=(b+c)/2} = 0 \tag{8}$$

for S-A modes
$$\left. \frac{dH_m(\xi)}{d\xi} \right|_{\xi=0} = H_m(\xi)|_{\xi=(b+c)/2} = 0 \tag{9}$$

for A-S modes
$$H_m(\xi)|_{\xi=0} = \frac{dH_m(\xi)}{d\xi}\bigg|_{\xi=(b+c)/2} = 0 \quad (10)$$

and for A-A modes
$$H_m(\xi)|_{\xi=0} = H_m(\xi)|_{\xi=(b+c)/2} = 0 \quad (11)$$

The admissible functions for the z -direction can be defined for several classical boundary conditions along the top and bottom edges of the tank; for the case of the clamped boundary condition at both edges

$$F_n(z)|_{z=0} = \frac{dF_n(z)}{dz}\bigg|_{z=0} = F_n(z)|_{z=a} = \frac{dF_n(z)}{dz}\bigg|_{z=a} = 0 \quad (12)$$

For the clamped-free boundary condition, the slope and deformation at the bottom edge must be zero, simultaneously. At the same time, the bending moments and shear forces at the top edge of the tank must disappear. Thus

$$F_n(z)|_{z=0} = \frac{dF_n(z)}{dz}\bigg|_{z=0} = \frac{d^2F_n(z)}{dz^2}\bigg|_{z=a} = \frac{d^3F_n(z)}{dz^3}\bigg|_{z=a} = 0 \quad (13)$$

When the top and bottom edges of the tank are simply supported, the displacements and bending moments must be zero

$$F_n(z)|_{z=0} = \frac{d^2F_n(z)}{dz^2}\bigg|_{z=0} = F_n(z)|_{z=a} = \frac{d^2F_n(z)}{dz^2}\bigg|_{z=a} = 0 \quad (14)$$

The first normalized polynomials of the ξ -axis can be derived from a set of boundary conditions written in Eqs. (8)-(11). For S-S modes

$$H_1(\xi) = \left\{ \frac{(b+3c)b^2}{16} - \frac{3}{4}(b+c)\xi^2 + \xi^3 \right\} G_1 \quad (15)$$

for S-A modes
$$H_1(\xi) = \left\{ \frac{b^2(b+c)^2}{8(2b+c)} - \frac{3b^2+3bc+c^2}{2(2b+c)}\xi^2 + \xi^3 \right\} G_1 \quad (16)$$

for A-S modes
$$H_1(\xi) = \left\{ \frac{b(b+c)(b+3c)}{4(b+2c)}\xi - \frac{2b^2+6bc+3c^2}{2(b+2c)}\xi^2 + \xi^3 \right\} G_1 \quad (17)$$

and for A-A modes
$$H_1(\xi) = \left\{ \frac{b(b+c)}{4}\xi - \frac{2b+c}{2}\xi^2 + \xi^3 \right\} G_1 \quad (18)$$

in which G_1 is a constant for the normalization. The generalized constant for the normalization is given as

$$G_m = \sqrt{\int_0^{(b+c)/2} \{H_m(\xi)\}^2 d\xi}, \quad m = 1, 2, 3 \dots \quad (19)$$

The successive polynomials can be generated from the recursive formulas based on the Gram-

Schmidt process (Dickinson and Di Blasio 1986, Cupial 1997) when a zero slope boundary condition need not be preserved at the boundary.

$$H_2(\xi) = (\xi - K_2)H_1(\xi) \tag{20}$$

$$H_p(\xi) = (\xi - K_p)H_{p-1}(\xi) - L_p H_{p-2}(\xi), \quad p = 3, 4, \dots \tag{21}$$

where

$$K_p = \frac{\int_0^{(b+c)/2} \xi \{H_{p-1}(\xi)\}^2 d\xi}{\int_0^{(b+c)/2} \{H_{p-1}(\xi)\}^2 d\xi}, \quad L_p = \frac{\int_0^{(b+c)/2} \xi H_{p-1}(\xi) H_{p-2}(\xi) d\xi}{\int_0^{(b+c)/2} \{H_{p-2}(\xi)\}^2 d\xi} \tag{22, 23}$$

To simulate the clamped edges at the top and bottom of the tank, the recurrence formulas of Eqs. (20) and (21) for the generation of the higher terms, $F_p(z)$, should be modified to preserve the zero slope boundary condition in addition to the zero displacement boundary condition at both ends. Therefore, it is necessary to use a modified version of the recurrence formulas of Eqs. (20) and (21), as written by Eqs. (24) and (25).

$$F_2(z) = (2z^3 - 3z^2 - K_2)F_1(z) \tag{24}$$

$$F_p(z) = (2z^3 - 3z^2 - K_p)F_{p-1}(z) - L_p F_{p-2}(z), \quad p = 3, 4, \dots \tag{25}$$

where

$$K_p = \frac{\int_0^a (2z^3 - 3z^2) \{F_{p-1}(z)\}^2 dz}{\int_0^a \{F_{p-1}(z)\}^2 dz}, \quad p = 3, 4, \dots \tag{26}$$

$$L_p = \frac{\int_0^a (2z^3 - 3z^2) F_{p-1}(z) F_{p-2}(z) dz}{\int_0^a \{F_{p-2}(z)\}^2 dz}, \quad p = 3, 4, \dots \tag{27}$$

The normalized orthogonal polynomials in the ξ -direction are obtained by the recursive formulas. All the displacement of the orthogonal admissible functions is zero at $\xi = (a + b)/2$ to simulate the vertical edges of the tank. Although the tank with the simply supported boundary condition may be formulated using a simple sinusoidal function in the vertical direction, the liquid motion in the tank cannot be described as an appropriate sinusoidal function satisfying simultaneously both the compatibility requirement along the wet surface and the liquid boundary condition at the bottom of the tank. Therefore, the polynomial functions, as admissible functions, are appropriate for the liquid-filled tank with the simply supported boundary condition instead of the sinusoidal function. Similarly, the first polynomial of the z -axis for the clamped boundary condition at both ends can be determined as

$$F_1(z) = 3\sqrt{70}(z^2 - 2z^3 + z^4) \tag{28}$$

The successive orthogonal polynomials can be generated from the recursive formulas based on the modified Gram-Schmidt processes of Eqs. (24)-(27). The first normalized polynomials of the z -axis for the other boundary conditions are given as

$$F_1(z) = \sqrt{30}[z^2 - z] \text{ for the simply supported boundary condition, and} \quad (29)$$

$$F_1(z) = \sqrt{45/104}[6z^2 - 4z^3 + z^4] \text{ for the clamped-free boundary condition} \quad (30)$$

2.3 Natural frequencies of dry rectangular tanks

The out-of-phase and in-phase modes are obviously symmetric and antisymmetric with respect to $x = 0$ and $y = 0$, not only for the dry tanks but also for the liquid-filled ones, since the tanks and liquid are symmetric in conjunction with the geometry and boundary conditions, as shown in Fig. 2. The symmetric dry or wet vibrational modes can only be obtained by a combination of the symmetric admissible functions. In the same way, the antisymmetric modes can only be constructed by a combination of the antisymmetric admissible functions. A sufficiently large finite number of terms, N and M , must be considered to obtain a converged solution, and a vector \mathbf{q} of the unknown coefficients is introduced to perform numerical calculations

$$\mathbf{q} = \{q_{11} \ q_{12} \ q_{13} \cdots q_{1N} \ q_{21} \ q_{22} \ q_{23} \cdots q_{MN}\}^T \quad (31)$$

where N indicates the number of admissible functions in the vertical direction (z) to be considered, and M represents those in the lateral direction (ξ).

To begin with, the kinetic and potential energies of the system should be defined to apply the Rayleigh-Ritz method using the admissible functions previously mentioned. The reference kinetic energy T^* , corresponding to a quarter of the rectangular tank, can be obtained by using the orthogonal property of the admissible functions

$$T^* = \frac{\rho h}{2} \mathbf{q}^T \mathbf{Z} \mathbf{q} \quad (32)$$

where ρ is the mass density of the rectangular tank. The matrix \mathbf{Z} in Eq. (32) is an $(MN) \times (MN)$ diagonal matrix which can be given as

$$Z = \int_0^a \int_0^{(b+c)/2} W_{mn} W_{uv} d\xi dz \quad (33)$$

The maximum potential energy V of a quarter of the rectangular tank can be computed by integrating the derivatives of the admissible modal functions

$$\begin{aligned} V = & \frac{D}{2} \int_0^a \int_0^{(b+c)/2} \left[\left\{ \frac{\partial^2 W_{mn}}{\partial \xi^2} \frac{\partial^2 W_{uv}}{\partial \xi^2} \right\} + \left\{ \frac{\partial^2 W_{mn}}{\partial z^2} \frac{\partial^2 W_{uv}}{\partial z^2} \right\} \right. \\ & \left. + \mu \left\{ \frac{\partial^2 W_{mn}}{\partial \xi^2} \frac{\partial^2 W_{uv}}{\partial z^2} + \frac{\partial^2 W_{uv}}{\partial \xi^2} \frac{\partial^2 W_{mn}}{\partial z^2} \right\} + 2(1-\mu) \left\{ \frac{\partial^2 W_{mn}}{\partial \xi \partial z} \frac{\partial^2 W_{uv}}{\partial \xi \partial z} \right\} \right] d\xi dz \quad (34) \end{aligned}$$

where the flexural rigidity of the tank is given as $D = Eh^3/12(1-\mu^2)$. The constants, m and E are the Poisson's ratio of the tank and modulus of elasticity, respectively. Inserting the orthogonal admissible functions into Eq. (34) gives the maximum potential energy of a quarter of the rectangular tank in a matrix form

$$V = \frac{D}{2} \mathbf{q}^T \mathbf{U} \mathbf{q} \tag{35}$$

where \mathbf{U} is also an $(MN) \times (MN)$ matrix that can be derived as

$$U = \Lambda 1_{mu} \Xi 1_{nv} + \Lambda 2_{mu} \Xi 2_{nv} + 2\mu \Lambda 3_{mu} \Xi 3_{nv} + 2(1 - \mu) \Lambda 4_{mu} \Xi 4_{nv} \tag{36}$$

and

$$\Lambda 1_{mu} = \int_0^{(b+c)/2} H_m''(\xi) H_u''(\xi) d\xi, \quad \Xi 1_{nv} = \int_0^a F_n(z) F_v(z) dz \tag{37, 38}$$

$$\Lambda 2_{mu} = \int_0^{(b+c)/2} H_m(\xi) H_u(\xi) d\xi, \quad \Xi 2_{nv} = \int_0^a F_n''(z) F_v''(z) dz \tag{39, 40}$$

$$\Lambda 3_{mu} = \int_0^{(b+c)/2} H_m''(\xi) H_u(\xi) d\xi, \quad \Xi 3_{nv} = \int_0^a F_n(z) F_v''(z) dz \tag{41, 42}$$

$$\Lambda 4_{mu} = \int_0^{(b+c)/2} H_m'(\xi) H_u'(\xi) d\xi, \quad \Xi 4_{nv} = \int_0^a F_n'(z) F_v'(z) dz \tag{43, 44}$$

where the apostrophe (') in the above equations indicates a derivative with respect to the corresponding variable. The relationship between the reference kinetic energy multiplied by its square circular frequency and maximum potential energy is used to extract the natural frequencies of the dry tank. The Rayleigh quotient for the dry rectangular tank is given as V/T^* . Minimizing the Rayleigh quotient with respect to the unknown parameters \mathbf{q} , the non-dimensional Galerkin equation yields

$$D\mathbf{U}\mathbf{q} - \omega^2 \rho h \mathbf{Z}\mathbf{q} = \{0\} \tag{45}$$

2.4 Displacement potential of the liquid

Since an ideal liquid partially contained in the rectangular tanks is assumed to be incompressible, inviscid, and irrotational, the velocity potential of the liquid can be given as the Laplace equation in the Cartesian coordinate

$$\nabla^2 \Phi(x, y, z, t) = \frac{\partial^2 \Phi}{\partial x^2} + \frac{\partial^2 \Phi}{\partial y^2} + \frac{\partial^2 \Phi}{\partial z^2} = 0 \tag{46}$$

For convenient formulation, the velocity potential Φ is separated into the harmonic time and space functions of the displacement potential, ϕ

$$\Phi(x, y, z, t) = i\omega \phi(x, y, z) \exp(i\omega t) \tag{47}$$

The vertical liquid displacement at $z = 0$ should vanish because the bottom wall of the tanks is rigid.

$$\left. \frac{\partial \phi(x, y, z)}{\partial z} \right|_{z=0} = 0 \tag{48}$$

When the gravity effect on the liquid-coupled system is neglected, the displacement potential at the free surface will be zero

$$\phi(x, y, z)|_{z=d} = 0 \tag{49}$$

We can get some important information from the dynamic symmetry of the liquid-coupled system.

The S-S modes requires zero liquid displacement along $x = 0$ and $y = 0$. Thus

$$\left. \frac{\partial \phi(x, y, z)}{\partial x} \right|_{x=0} = \left. \frac{\partial \phi(x, y, z)}{\partial y} \right|_{y=0} = 0 \quad (50)$$

The displacement potential satisfying both the Laplace equation of Eq. (46) and the boundary condition of Eqs. (48)-(50) can be written as

$$\phi(x, y, z) = \sum_{r=1}^{\infty} \sum_{s=1}^{\infty} [R_{rs} \cosh(\alpha_{rs} x) \cos(\beta_s y) + G_{rs} \cos(\tau_s x) \cosh(\sigma_{rs} y)] \cos(\lambda_r z) \quad (51)$$

where

$$\beta_s = \frac{2(s-1)\pi}{c}, \tau_s = \frac{2(s-1)\pi}{b}, \lambda_r = \frac{(2r-1)\pi}{2d} \quad (52-54)$$

$$\alpha_{rs} = \sqrt{\beta_s^2 + \lambda_r^2}, \sigma_{rs} = \sqrt{\tau_s^2 + \lambda_r^2}, s, r = 1, 2, 3, \dots \quad (55, 56)$$

where R_{rs} and G_{rs} are unknown coefficients that can be determined by the compatibility condition at the wet surface between the tank and liquid. The liquid boundary conditions and corresponding displacement potentials for S-A, A-S and A-A modes are summarized in Appendix A.

Along the liquid-contacting surfaces, the transverse displacement of the tank must be identical to the dynamic liquid displacement normal to the interface surface, and thus the compatibility conditions yield the following for the S-S modes

$$\sum_{m=1}^M \sum_{n=1}^N q_{mn} W_{mn}(\xi, z) = \left[\frac{\partial \phi(x, y, z)}{\partial y} \right]_{y=c/2} \quad \text{for } 0 \leq z \leq d \text{ and } 0 \leq \xi \leq b/2 \quad (57)$$

$$\sum_{m=1}^M \sum_{n=1}^N q_{mn} W_{mn}(\xi, z) = \left[\frac{\partial \phi(x, y, z)}{\partial x} \right]_{x=b/2} \quad \text{for } 0 \leq z \leq d \text{ and } b/2 \leq \xi \leq (b+c)/2 \quad (58)$$

where $x = \xi$ for $0 \leq \xi \leq b/2$ and $y = -\xi + (b+c)/2$ for $b/2 \leq \xi \leq (b+c)/2$.

Substituting Eqs. (2) and (51) into Eqs. (57) and (58) results in

$$\sum_{n=1}^N \sum_{m=1}^M q_{mn} H_m(\xi) F_n(z) = \sum_{r=1}^{\infty} \sum_{s=1}^{\infty} \sigma_{rs} G_{rs} \sinh\left(\frac{\sigma_{rs} c}{2}\right) \cos(\tau_s x) \cos(\lambda_r z) \quad (59)$$

$$\sum_{n=1}^N \sum_{m=1}^M q_{mn} H_m(\xi) F_n(z) = \sum_{r=1}^{\infty} \sum_{s=1}^{\infty} \alpha_{rs} R_{rs} \sinh\left(\frac{\alpha_{rs} b}{2}\right) \cos(\beta_s y) \cos(\lambda_r z) \quad (60)$$

Multiplication of $\sum_{r=1}^{\infty} \sum_{s=1}^{\infty} \cos(\tau_s x) \cos(\lambda_r z)$ and $\sum_{r=1}^{\infty} \sum_{s=1}^{\infty} \cos(\beta_s y) \cos(\lambda_r z)$ into Eqs. (59) and (60),

respectively, and integration along the wet surfaces to perform the finite Fourier transform, give relationships between the unknown coefficients for the S-S modes

$$R_{rs} = \sum_{n=1}^N \sum_{m=1}^M \frac{q_{mn} \Omega_{ms} \Lambda_{nr}}{\alpha_{rs} C_s \sinh(\alpha_{rs} b/2) J_r}, \quad G_{rs} = \sum_{n=1}^N \sum_{m=1}^M \frac{q_{mn} \Gamma_{ms} \Lambda_{nr}}{\sigma_{rs} D_s \sinh(\sigma_{rs} c/2) J_r} \quad (61, 62)$$

where the parameters Ω_{ms} , Λ_{nr} , C_s , D_s and J_r are defined in Appendix A. Now, the displacement

potential can be described in terms of the unknown coefficients, q_{mn} , in the admissible functions of the tanks. For the other modes, the unknown coefficients, R_{rs} and G_{rs} , can be determined by the same process as described in Appendix A.

2.5 Natural frequencies of wet rectangular tanks

As the reference kinetic energy of the liquid in the tanks for the S-S modes can be evaluated from its boundary motion, the reference kinetic energy of the liquid is given as

$$T_o^* = -\frac{V1}{2}\rho_o \sum_{u=1}^M \sum_{v=1}^N \left\{ \int_0^{b/2} \int_0^d W_{uv} q_{uv} \phi(x, c/2, z) dx dz + \int_0^{c/2} \int_0^d W_{uv} q_{uv} \phi(b/2, y, z) dy dz \right\} \quad (63)$$

where ρ_o is the mass density of the contained liquid. By substituting Eqs. (2), (51), (61) and (62) into Eq. (63), one can obtain

$$T_o^* = \frac{1}{2}\rho_o \sum_{m=1}^M \sum_{n=1}^N \sum_{u=1}^M \sum_{v=1}^N q_{uv} q_{mn} \sum_{r=1}^\infty \sum_{s=1}^\infty \left[\frac{\Omega_{ms}}{\alpha_{rs} C_s} \left\{ \frac{\chi_{urs} (-1)^{s+1}}{\sinh(\alpha_{rs} b/2)} + \frac{\Omega_{us}}{\tanh(\alpha_{rs} b/2)} \right\} + \frac{\Gamma_{ms}}{\sigma_{rs} D_s} \left\{ \frac{\Gamma_{us}}{\tanh(\sigma_{rs} c/2)} + \frac{\theta_{usr} (-1)^{s+1}}{\sinh(\sigma_{rs} c/2)} \right\} \right] \frac{\Lambda_{nr} \Lambda_{vr}}{J_r} = \rho_o \mathbf{q}^T \mathbf{G} \mathbf{q} \quad (64)$$

where the coefficients, χ_{urs} and θ_{urs} , are defined in Appendix A. By the same method, for the S-A modes, A-S modes, and A-A modes, the reference kinetic energy of the contained liquid can be formulated as listed in Appendix A.

The reference total kinetic energy multiplied by its square circular frequency should be equal to the maximum potential energy of the liquid-coupled system. Minimizing the Rayleigh quotient with respect to the unknown parameters, \mathbf{q} , eventually the eigenvalue equation is obtained, and the wet natural frequencies can be calculated by making the determinant of Eq. (65) zero.

$$DU\mathbf{q} - \omega^2 \{ \rho \mathbf{Z} + \rho_o \mathbf{G} \} \mathbf{q} = \{ 0 \} \quad (65)$$

3. Examples and discussion

3.1 Examples for theoretical calculation and finite element analysis

The eigenvalues of Eq. (65) were calculated using commercial software, Mathcad, (version 14) in order to find the natural frequencies of rectangular tanks partially filled with water. The frequency equation derived in the previous sections involves infinite series expansions of algebraic terms and a finite number of admissible functions. In the theoretical calculation, the series expansion terms r and s were set at 30, and the numbers of admissible functions were 10 in the ξ -direction and 10 in the z -direction regardless of the symmetry of the vibrational modes, which gave converged solutions.

In order to check the validity of the proposed theory, three-dimensional finite element analyses were also carried out for the liquid-coupled system using a commercial computer code, ANSYS (release 10.0). Finite element models were constructed with the tank geometry, boundary conditions, and material properties used in the theoretical calculation. The aluminum tank was 360 mm in

height, 300 mm in length, 240 mm in width, and 3 mm in thickness. The liquid depth in the z -direction was considered for two water levels, that is, $d = 0$ mm (dry condition) and $d = 180$ mm (50% water level). The physical properties of the aluminum tank material were as follows: modulus of elasticity = 69.0 GPa, Poisson's ratio = 0.3 and mass density = 2700 kg/m³. The liquid contained in the tanks had a density of 1000 kg/m³. The viscosity and compressibility of water were neglected in both the theoretical calculations and finite element analyses.

Finite element analyses using a commercial computer code, ANSYS software (release 11), were performed to obtain the natural frequencies and mode shapes of the rectangular tanks partially filled with water for the several boundary conditions as mentioned above. Three-dimensional finite element models were constructed with contained fluid elements (FLUID80) and elastic shell elements (SHELL63) of ANSYS software. The liquid movement along the bottom rigid wall was restricted to the vertical direction only to realize Eq. (48). The displacement of the liquid element nodes adjacent to the surface of the wetted rectangular tanks coincided to that of the rectangular tanks so that the finite element model can simulate Eqs. (57) and (58) in the range of $0 \leq z \leq d$. The smaller facing rectangular plates of the tanks were divided into 2880 (48×60) elastic shell elements with the same size, and the larger facing rectangular plates were divided into 4320 (72×60) elastic shell elements with the same size. Therefore, the total number of shell elements for the tanks was 14400. On the other hand, the liquid region of the finite element model consisted of 103680 ($36 \times 60 \times 48$) fluid elements with an identical size to build a 50% liquid depth ratio. Several classical boundary conditions were considered such as clamped, simply supported, and clamped-free boundary conditions along the top and bottom edges of the tanks in the finite element model. The total number of 50 modal frequencies and corresponding mode shapes were extracted and plotted in the finite element analyses, which employs the Block Lanczos method.

3.2 Comparison of theoretical and finite element results

The theoretical natural frequencies of the rectangular tanks for the dry condition are listed and

Table 1 Natural frequencies of a dry rectangular tank with the clamped boundary condition at both ends

Serial mode	Mode		Natural frequency (Hz)		Discrepancy (%)
	x - z plane	y - z plane	Theory	ANSYS	
1	S (0,0)	S (0,0)	193.6	193.5	0.05
2	S (0,0)	A (1,0)	214.0	213.5	0.23
3	A (1,0)	S (0,0)	263.2	262.4	0.31
4	S (0,0)	S (0,0)	301.7	301.2	0.17
5	S (0,1)	S (0,1)	419.8	419.6	0.05
6	S (0,1)	A (1,1)	429.4	429.0	0.09
7	A (1,0)	A (1,0)	454.9	446.0	2.00
8	A (1,1)	S (0,1)	478.0	477.4	0.13
9	S (0,1)	S (0,1)	498.6	497.8	0.16
10	A (1,0)	S (0,0)	505.0	498.0	1.41

Note : The symbol "A" represents antisymmetric modes and the symbol "S" indicates symmetric modes. The numbers indicate the number of nodal lines.

Table 2 Natural frequencies of the dry rectangular tank with the simply supported boundary condition at both ends

Serial Mode	Mode		Natural frequency (Hz)		Discrepancy (%)
	<i>x-z</i> plane	<i>y-z</i> plane	Theory	ANSYS	
1	S (0,0)	S (0,0)	149.6	149.6	0.00
2	S (0,0)	A (1,0)	175.4	174.5	0.52
3	A (1,0)	S (0,0)	230.2	228.7	0.66
4	S (0,0)	S (0,0)	273.7	273.2	0.18
5	S (0,1)	S (0,1)	314.1	314.0	0.03
6	S (0,1)	A (1,1)	326.9	326.3	0.18
7	A (1,1)	S (0,1)	384.0	383.1	0.24
8	S (0,1)	S (0,1)	409.6	408.8	0.20
9	A (1,0)	A (1,0)	432.2	421.4	2.56
10	A (1,0)	S (2,0)	484.9	477.3	1.59

Note : The symbol “A” represents antisymmetric modes and the symbol “S” indicates symmetric modes. The numbers indicate the number of nodal lines.

Table 3 Natural frequencies of the dry rectangular tank with the clamped-free boundary condition

Serial mode	Mode		Natural frequency (Hz)		Discrepancy (%)
	<i>x-z</i> plane	<i>y-z</i> plane	Theory	ANSYS	
1	S (0,0)	S (0,0)	109.6	109.8	-0.18
2	S (0,0)	A (1,0)	142.9	142.0	0.63
3	A (1,0)	S (0,0)	194.3	192.3	1.04
4	S (0,1)	S (0,1)	224.5	224.6	-0.05
5	S (0,1)	A (1,1)	242.2	241.9	0.12
6	S (0,0)	S (0,0)	245.6	244.6	0.41
7	A (1,1)	S (0,1)	298.6	299.1	-0.17
8	S (0,1)	S (0,1)	331.9	332.3	-0.12
9	A (1,0)	A (1,0)	392.6	378.4	3.75
10	A (1,0)	S (2,0)	450.9	441.1	2.22

Note : The symbol “A” represents antisymmetric modes and the symbol “S” indicates symmetric modes. The numbers indicate the number of nodal lines.

compared with the finite element analysis results in Tables 1~3 for the clamped, simply supported, and clamped-free boundary conditions, respectively. The number in the tables indicates the number of nodal lines with respect to the lateral and vertical directions.

It was found that the discrepancies between the theoretical and finite element analyses results are less than approximately 4% within the 10th serial mode for the dry condition. These results indicate that the combination of orthogonal polynomials can appropriately approximate the mode shapes of the dry rectangular tank for such classical boundary conditions. Since each mode shape is symmetric or

Table 4 Natural frequencies of the clamped rectangular tank filled with water (50% water level)

Serial mode	Mode		Natural frequency (Hz)		Discrepancy (%)
	$x-z$ plane	$y-z$ plane	Theory	ANSYS	
1	S (0,0)	S (0,0)	93.2	92.9	-0.32
2	S (0,0)	A (1,0)	104.5	104.2	-0.29
3	S (0,0)	S (0,0)	124.5	120.8	-3.06
4	A (1,0)	S (0,0)	131.0	128.5	-1.91
5	A (1,0)	S (0,1)	246.0	225.0	-3.66
6	A (1,0)	A (1,0)	232.7	232.8	0.04
7	S (0,1)	S (0,1)	279.8	275.7	-1.48
8	S (0,1)	A (1,0)	276.9	276.1	-1.03
9	S (2,0)	S (0,1)	319.9	316.6	-1.04
10	A (1,1)	S (0,1)	337.6	327.0	-3.06

Note : The symbol "A" represents antisymmetric modes and the symbol "S" indicates symmetric modes. The numbers indicate the number of nodal lines.

Table 5 Natural frequencies of the simply supported rectangular tank filled with water (50% water level)

Serial mode	Mode		Natural frequency (Hz)		Discrepancy (%)
	$x-z$ plane	$y-z$ plane	Theory	ANSYS	
1	S (0,0)	S (0,0)	69.1	68.5	-0.87
2	S (0,0)	A (1,0)	80.0	79.7	-0.37
3	S (0,0)	S (0,0)	99.8	97.1	-2.78
4	A (1,0)	S (0,0)	107.8	104.7	-2.96
5	A (1,0)	S (0,1)	222.0	201.0	-10.44
6	A (1,0)	A (1,0)	204.1	209.7	2.67
7	S (0,1)	S (0,1)	215.5	212.2	-1.55
8	S (0,1)	A (1,0)	217.8	216.7	-0.51
9	S (2,1)	S (0,1)	269.3	267.5	-0.67
10	A (1,1)	S (0,1)	278.6	270.3	-3.07

Note : The symbol "A" represents antisymmetric modes and the symbol "S" indicates symmetric modes. The numbers indicate the number of nodal lines.

antisymmetric with respect to $y = b/2$ or $x = a/2$, the admissible functions were selected from the corresponding symmetric and antisymmetric modes so that the matrix sizes in the theoretical calculation could be reduced.

The natural frequencies of the rectangular tanks filled with water for the liquid depth $d = 180$ mm are listed in Tables 4~6 within the 10th serial modes for the typical boundary conditions. It was found that the theoretical wet natural frequencies agreed well with the finite element results within approximately a 4% error range for the 50% liquid level, except one mode with the simply

Table 6 Natural frequencies of the clamped–free rectangular tank filled with water (50% water level)

Serial mode	Mode		Natural frequency (Hz)		Discrepancy (%)
	<i>x</i> - <i>z</i> plane	<i>y</i> - <i>z</i> plane	Theory	ANSYS	
1	S (0,0)	S (0,0)	84.2	82.8	1.66
2	S (0,0)	A (1,0)	99.1	98.2	0.91
3	S (0,1)	S (0,0)	111.7	111.5	0.18
4	A (1,0)	S (0,0)	127.5	125.1	1.88
5	S (0,1)	S (0,1)	146.9	145.7	0.82
6	S (0,1)	A (1,0)	159.5	160.4	-0.56
7	A (1,0)	S (0,1)	202.6	202.4	0.10
8	A (1,0)	A (1,0)	227.0	231.4	-0.94
9	A (1,1)	S (0,1)	251.3	243.7	3.02
10	S (0,0)	S (0,1)	249.3	248.8	0.20

Note : The symbol “A” represents antisymmetric modes and the symbol “S” indicates symmetric modes. The numbers indicate the number of nodal lines.

supported boundary condition, and that most of the theoretical natural frequencies overestimated the finite element results slightly. It was observed that the wet natural frequencies decrease with the water depth due to an increase of hydrodynamic mass, as is well known.

3.3 Mode shapes

The typical dry and wet mode shapes of the tanks with 50% water level were illustrated in Figs. 4~9 for the various boundary conditions. Figs. 4~6 show the dry mode shapes of the rectangular tanks with the clamped, simply supported, and clamped-free boundary conditions, respectively. The dry mode shapes of each plate in the tanks are almost identical to the dry mode shapes of a single plate. However, the relative deformations of connected neighboring plates are not identical to each other due to the difference in the flexural rigidity between the neighboring plates of the tanks. It could be noted that the wet mode shapes of the tanks are slightly distorted from the classical dry mode shapes of the rectangular plates due to the hydrodynamic effect of water. In particular, it was found that the higher wet mode shapes are too severely distorted from the corresponding dry mode shapes. The dry and wet mode shapes of the clamped tank are very similar to those of the simply supported tank, as shown in Figs. 4, 5, 7, and 8. Just as the mode shapes of a clamped uniform beam are similar to those of a simply supported beam, the mode shapes of the clamped tank resembled those of the simply supported tank.

In the rectangular tanks, two apparently similar modes, not only the 1st and 4th modes in Figs. 4 and 5, but also the 1st and 3rd modes in Fig. 7 and 8, were observed in the S-S modes. Although these two simplest mode shapes had zero nodal lines in width and length, they had different phases. The fundamental mode in Figs. 5 and 6 showed an out-of-phase mode of an oval type; on the other hand, the 4th mode showed an out-of-phase mode of a bulging type. That is, the fundamental mode shapes in Figs. 4, 5, 7, and 8 correspond to a typical mode with a circumferential wave number $n = 2$ in a circular cylindrical shell. However, the 4th mode shapes in Figs. 4 and 5 correspond to the

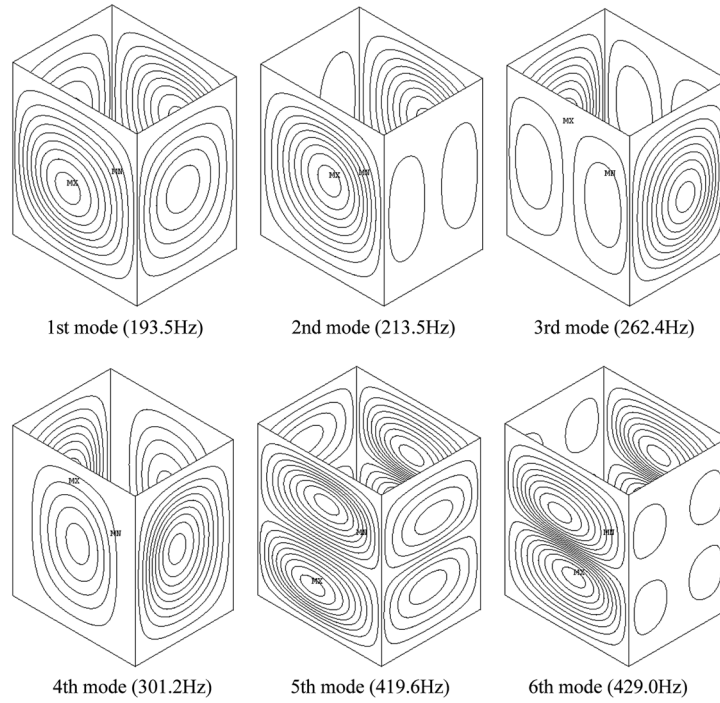


Fig. 4 Mode shapes of a dry rectangular tank with the clamped boundary condition at both ends

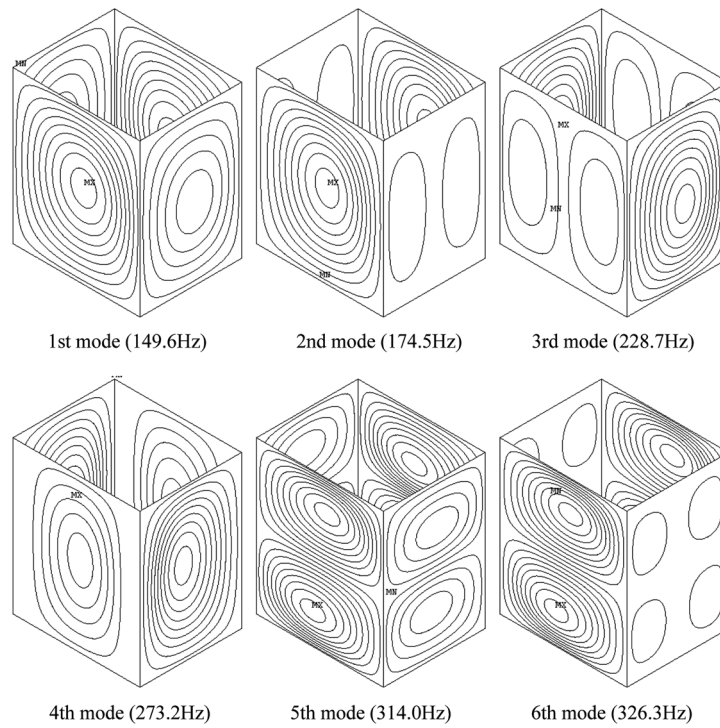


Fig. 5 Mode shapes of a dry rectangular tank with the simply supported boundary condition at both ends

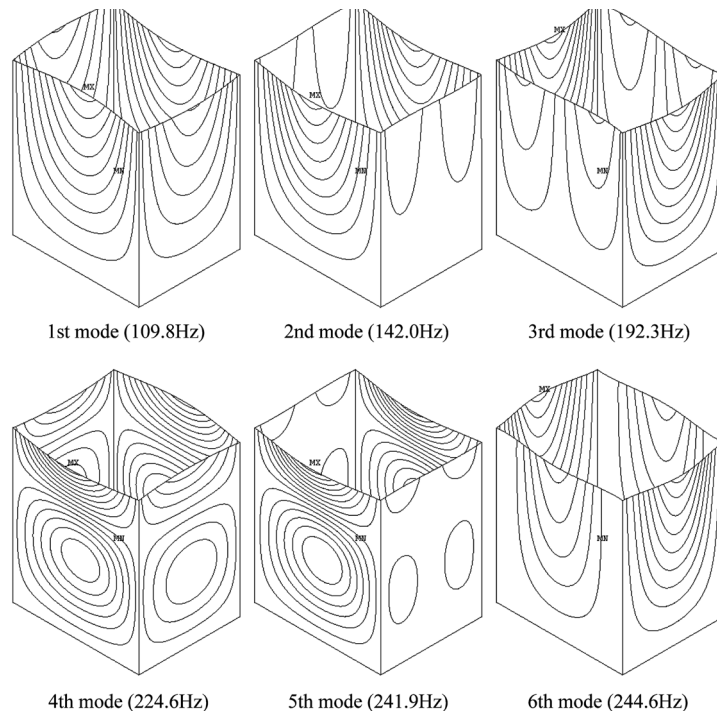


Fig. 6 Mode shapes of a dry rectangular tank with the clamped-free boundary condition

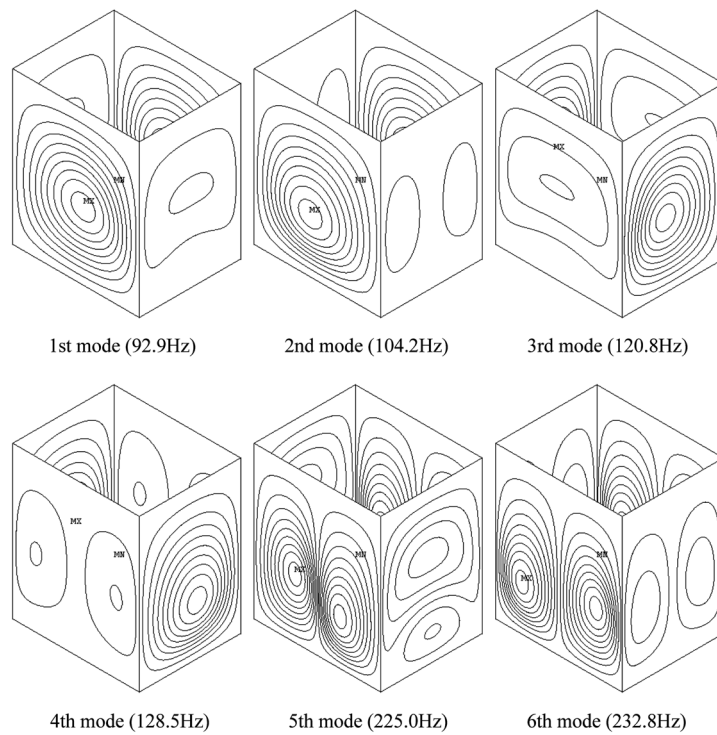


Fig. 7 Mode shapes of a clamped wet rectangular tank with a half liquid level

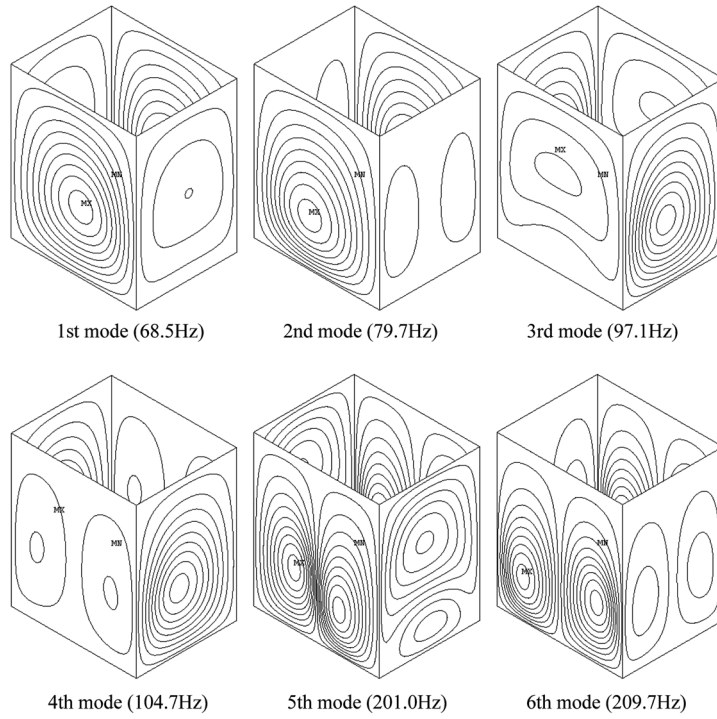


Fig. 8 Mode shapes of a simply supported wet rectangular tank with a half liquid level

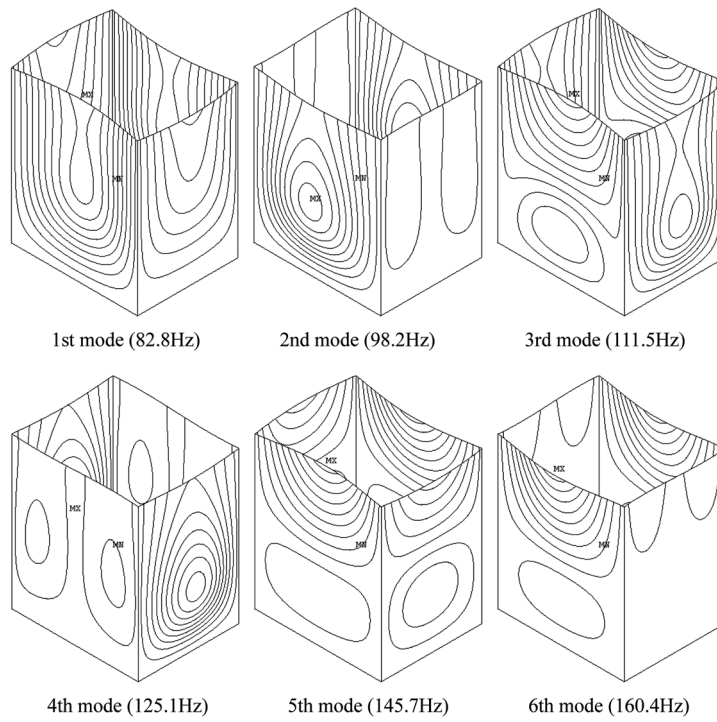


Fig. 9 Mode shapes of a clamped-free wet rectangular tank with a half liquid level

typical mode shape with the circumferential wave number $n = 0$ in the circular cylindrical shell. This explains why the fundamental natural frequency of the tank is lower than the 4th natural frequency in Figs. 4 and 5. Generally, it was observed that the discrepancies between the theoretical natural frequencies and those of the finite element analyses for the antisymmetric modes were slightly larger than those for the symmetric modes. It is highly probable that the edge deformation of the tanks can appear in the finite element model, although the edge deformation is assumed to be zero in the theoretical formulation.

3.4 Liquid depth effect

It was observed that the mode shapes and natural frequencies change according to the liquid level. The wet fundamental natural frequencies of the tanks, which are all symmetric with respect to the centerlines, decrease to 48.0%, 45.8%, and 75.4% from those of dry tanks for the clamped, simply supported and clamped-free boundary conditions, respectively, when the liquid level is 50%. This shows that the hydrodynamic effect on the tank with a half-liquid level is largest for the simply supported boundary condition. However, the hydrodynamic effect on the tank will drastically increase when the liquid level changes from 50% to 100% for the clamped-free boundary condition.

As shown in Figs. 4 and 7, it is noted that the order of modes changed according to the liquid level. For example, the 3rd (A-S mode) and 4th serial modes (S-S mode) in the dry condition were

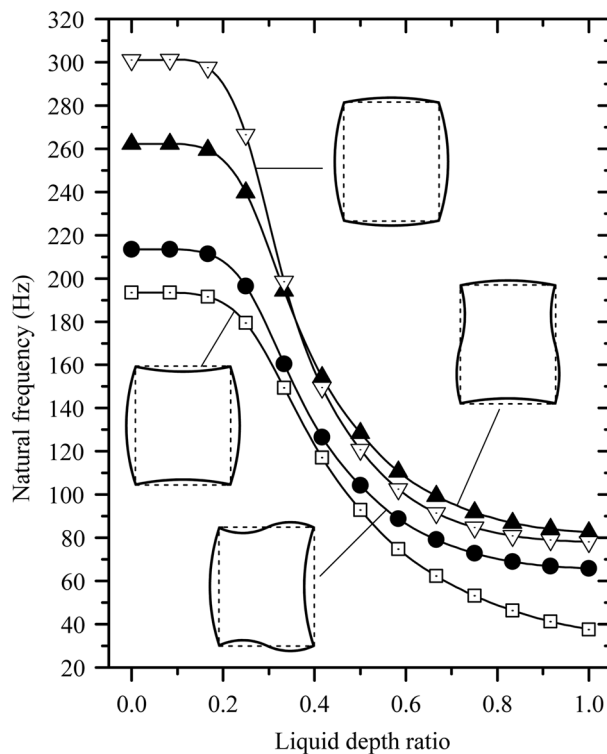


Fig. 10 Liquid depth effect on the natural frequencies of the clamped rectangular tank filled with water (—□—, S-S mode; —●—, A-S mode; —▲—, S-A mode; —▽—; S-S mode)

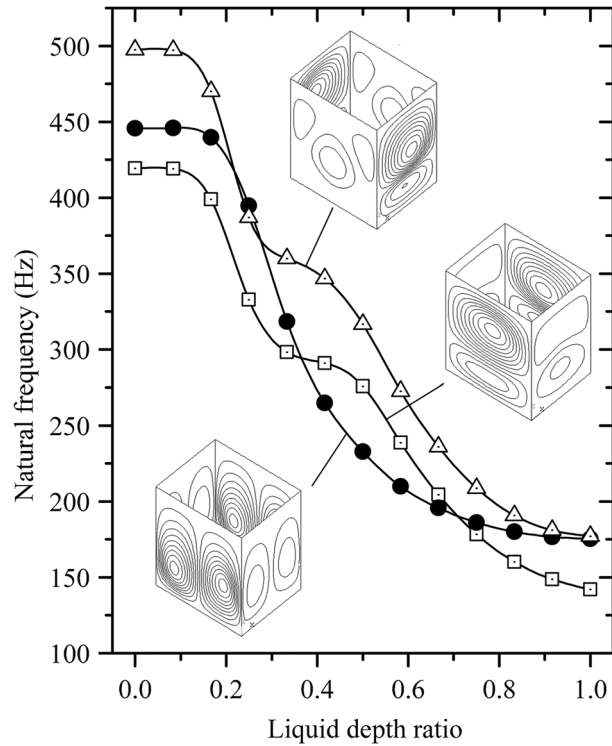


Fig. 11 Liquid depth effect on the natural frequencies of the clamped rectangular tank filled with water (—□—, S-S mode; —●—, A-A mode; —▲—, S-S mode)

switched to the 4th (A-S mode) and 3rd serial modes (S-S mode) in the wet condition, respectively, as shown in Figs. 4 and 7 for the clamped boundary condition. Figs. 10 and 11 illustrate the natural frequencies of the clamped tank as a function of the liquid depth ratio. All the natural frequencies of the tank decreased with the liquid depth, as is well known. The decrease of natural frequencies was not linear but *L* shaped for the modes with zero horizontal nodal line, as illustrated in Fig. 10. The effect of the number of horizontal nodal lines on the natural frequencies is shown in Fig. 11. We could observe that one horizontal nodal line in the modes of the clamped tank makes one transition plateau in Fig. 11. This is the same phenomenon as two rectangular plates partially coupled with a liquid (Jeong and Kim 2009), or a single circular shell partially filled with a liquid (Jeong and Lee 1998).

4. Conclusions

An analytical method based on the Rayleigh-Ritz approach for calculating natural frequencies of rectangular tanks partially contained with a liquid was developed for several classical boundary conditions of the tanks. The wet dynamic displacement of the tanks was approximated by combining the orthogonal polynomial functions satisfying the boundary conditions at the top and bottom edges of the tanks. The liquid displacement potentials satisfying the liquid boundary conditions and the Laplace equation were derived, and the wet dynamic modal functions of the tanks were expanded in

terms of the finite Fourier series for a compatibility requirement along the contacting surface between the tanks and liquid. From the appropriate liquid displacement potentials and admissible modal functions, the total kinetic and potential energies of the liquid coupled system were extracted. Finally, the Rayleigh-Ritz method led to an eigenvalue problem to calculate the wet natural frequencies of the rectangular tanks. The proposed analytical method was verified by observing an excellent agreement with three-dimensional finite element analysis results. It was shown that the dynamic characteristics of the partially liquid-filled tanks show a similarity to those of a circular cylindrical shell partially filled with water.

References

- Cheung, Y.K. and Zhou, D. (2000), "Coupled vibratory characteristics of a rectangular container bottom plate", *J. Fluid. Struct.*, **14**, 339-357.
- Cupial, P. (1997), "Calculation of the natural frequencies of composite plates by the Rayleigh-Ritz method with orthogonal polynomials", *J. Sound Vib.*, **201**, 385-387.
- Dickinson, S.M. and Di Blasio, A. (1986), "On the use of orthogonal polynomials in the Rayleigh-Ritz method for the study of the flexural vibration and buckling of isotropic and orthotropic rectangular plates", *J. Sound Vib.*, **108**, 51-62.
- Ergin, A. and Uğurlu, B. (2003), "Linear vibration analysis of cantilever plates partially submerged in fluid", *J. Fluid. Struct.*, **17**, 927-939.
- Hashemi, H.S., Karimi, M. and Taher, H.R.D. (2010), "Vibration analysis of rectangular Mindlin plates on elastic foundations and vertically in contact with stationary fluid by the Ritz method", *Ocean Eng.*, **37**, 174-185.
- Hashemi, H.S., Karimi, M. and Rokni, H.R. (2010), "Hydroelastic vibration and buckling of rectangular Mindlin plates on Pasternak foundations under linearly varying in-plane loads", *Soil Dyn. Earthq. Eng.*, **30**, 1487-1499.
- Jeong, K.H. and Lee, S.C. (1998), "Hydroelastic vibration of a liquid-filled circular cylindrical shell", *Comput. Struct.*, **66**, 173-185.
- Jeong, K.H., Yoo, G.H. and Lee, S.C. (2003), "Hydroelastic vibration of two identical rectangular plates", *J. Sound Vib.*, **272**, 539-555.
- Jeong, K.H. and Kim, J.W. (2009), "Hydroelastic vibration analysis of two flexible rectangular plates partially coupled with a liquid", *Nucl. Eng. Tech.*, **41**, 335-346.
- Kerboua, Y., Lakis, A.A., Thomas, M. and Marcouiller, L. (2008), "Vibration analysis of rectangular plates coupled with fluid", *Appl. Math. Model.*, **32**, 2570-2586.
- Liang, C.C., Liao, C.C., Tai, Y.S. and Lai, W.H. (2001), "The free vibration analysis of submerged cantilever plates", *Ocean Eng.*, **28**, 1225-1245.
- Uğurlu, B., Kutlu, A., Ergin, A. and Omurtag, M.H. (2008), "Dynamics of a rectangular plate resting on an elastic foundation and partially in contact with a quiescent fluid", *J. Sound Vib.*, **317**, 308-328.
- Yadykin, Y., Tenetov, V. and Levin, D. (2003), "The added mass of a flexible plate oscillating in a fluid", *J. Fluid. Struct.*, **17**, 115-123.
- Zhou, D. and Cheung, Y.K. (2000), "Vibration of vertical rectangular plate in contact with water on one side", *Earthq. Eng. Struct. Dyn.*, **29**, 693-710.
- Zhou, D. and Liu, W. (2007), "Hydroelastic vibrations of flexible rectangular tanks partially filled with liquid", *Int. J. Numer. Method. Eng.*, **71**, 149-174.

Appendix A: Displacement potentials and kinetic energies of liquid

A.1 Liquid boundary conditions

Mode	Description
S-S	$\left. \frac{\partial \phi(x, y, z)}{\partial x} \right _{x=0} = \left. \frac{\partial \phi(x, y, z)}{\partial y} \right _{y=0} = 0$
S-A	$\left. \frac{\partial \phi(x, y, z)}{\partial x} \right _{x=0} = 0, \quad \frac{\partial \phi(x, y, z)}{\partial y} = \frac{\partial \phi(x, -y, z)}{\partial y}$
A-S	$\frac{\partial \phi(x, y, z)}{\partial x} = \frac{\partial \phi(-x, y, z)}{\partial x}, \quad \left. \frac{\partial \phi(x, y, z)}{\partial y} \right _{y=0} = 0$
A-A	$\frac{\partial \phi(x, y, z)}{\partial x} = \frac{\partial \phi(-x, y, z)}{\partial x}, \quad \frac{\partial \phi(x, y, z)}{\partial y} = \frac{\partial \phi(x, -y, z)}{\partial y}$

A.2 Displacement potentials

Mode	Description
S-S	$\phi(x, y, z) = \sum_{r=1}^{\infty} \sum_{s=1}^{\infty} [R_{rs} \cosh(\alpha_{rs} x) \cos(\beta_s y) + G_{rs} \cos(\tau_r x) \cosh(\sigma_{rs} y)] \cos(\lambda_r z)$ $\beta_s = \frac{2(s-1)\pi}{c}, \tau_r = \frac{2(s-1)\pi}{b}, \lambda_r = \frac{(2r-1)\pi}{2d}, \alpha_{rs} = \sqrt{\beta_s^2 + \lambda_r^2}, \sigma_{rs} = \sqrt{\tau_r^2 + \lambda_r^2}$
S-A	$\phi(x, y, z) = \sum_{r=1}^{\infty} \sum_{s=1}^{\infty} [R_{rs} \cosh(\alpha_{rs} x) \sin(\beta_s y) + G_{rs} \cos(\tau_r x) \sinh(\sigma_{rs} y)] \cos(\lambda_r z)$ $\beta_s = \frac{(2s-1)\pi}{c}, \tau_r = \frac{2(s-1)\pi}{b}, \lambda_r = \frac{(2r-1)\pi}{2d}, \alpha_{rs} = \sqrt{\beta_s^2 + \lambda_r^2}, \sigma_{rs} = \sqrt{\tau_r^2 + \lambda_r^2}$
A-S	$\phi(x, y, z) = \sum_{r=1}^{\infty} \sum_{s=1}^{\infty} [R_{rs} \sinh(\alpha_{rs} x) \cos(\beta_s y) + G_{rs} \sin(\tau_r x) \cosh(\sigma_{rs} y)] \cos(\lambda_r z)$ $\beta_s = \frac{2(s-1)\pi}{c}, \tau_r = \frac{(2s-1)\pi}{b}, \lambda_r = \frac{(2r-1)\pi}{2d}, \alpha_{rs} = \sqrt{\beta_s^2 + \lambda_r^2}, \sigma_{rs} = \sqrt{\tau_r^2 + \lambda_r^2}$
A-A	$\phi(x, y, z) = \sum_{r=1}^{\infty} \sum_{s=1}^{\infty} [R_{rs} \sinh(\alpha_{rs} x) \sin(\beta_s y) + G_{rs} \sin(\tau_r x) \sinh(\sigma_{rs} y)] \cos(\lambda_r z)$ $\beta_s = \frac{(2s-1)\pi}{c}, \tau_r = \frac{(2s-1)\pi}{b}, \lambda_r = \frac{(2r-1)\pi}{2d}, \alpha_{rs} = \sqrt{\beta_s^2 + \lambda_r^2}, \sigma_{rs} = \sqrt{\tau_r^2 + \lambda_r^2}$

A.3 Coefficients in displacement potentials

Mode	Description	
S-S	$R_{rs} = \sum_{n=1}^N \sum_{m=1}^M \frac{q_{mn} \Omega_{ms} \Lambda_{nr}}{\alpha_{rs} C_s \sinh(\alpha_{rs} b/2) J_r}$	$G_{rs} = \sum_{n=1}^N \sum_{m=1}^M \frac{q_{mn} \Gamma_{ms} \Lambda_{nr}}{\sigma_{rs} D_s \sinh(\sigma_{rs} c/2) J_r}$
S-A	$R_{rs} = \sum_{n=1}^N \sum_{m=1}^M \frac{q_{mn} \varphi_{ms} \Lambda_{nr}}{\alpha_{rs} E_s \sinh(\alpha_{rs} b/2) J_r}$	$G_{rs} = \sum_{n=1}^N \sum_{m=1}^M \frac{q_{mn} \Gamma_{ms} \Lambda_{nr}}{\sigma_{rs} D_s \cosh(\sigma_{rs} c/2) J_r}$
A-S	$R_{rs} = \sum_{n=1}^N \sum_{m=1}^M \frac{q_{mn} \Omega_{ms} \Lambda_{nr}}{\alpha_{rs} C_s \cosh(\alpha_{rs} b/2) J_r}$	$G_{rs} = \sum_{n=1}^N \sum_{m=1}^M \frac{q_{mn} \varepsilon_{ms} \Lambda_{nr}}{\sigma_{rs} \Delta_s \sinh(\sigma_{rs} c/2) J_r}$
A-A	$R_{rs} = \sum_{n=1}^N \sum_{m=1}^M \frac{q_{mn} \varphi_{ms} \Lambda_{nr}}{\alpha_{rs} E_s \cosh(\alpha_{rs} b/2) J_r}$	$G_{rs} = \sum_{n=1}^N \sum_{m=1}^M \frac{q_{mn} \varepsilon_{ms} \Lambda_{nr}}{\sigma_{rs} \Delta_s \cosh(\sigma_{rs} c/2) J_r}$

A.4 Kinetic energies of liquid

Mode	Description
S-S	$\frac{1}{2} \rho_o \sum_{m=1}^M \sum_{n=1}^N \sum_{u=1}^M \sum_{v=1}^N q_{uv} q_{mn} \sum_{r=1}^{\infty} \sum_{s=1}^{\infty} \left[\frac{\Omega_{ms}}{\alpha_{rs} C_s} \left\{ \frac{\chi_{urs}(-1)^{s+1}}{\sinh(\alpha_{rs} b/2)} + \frac{\Omega_{us}}{\tanh(\alpha_{rs} b/2)} \right\} \right. \\ \left. + \frac{\Gamma_{ms}}{\sigma_{rs} D_s} \left\{ \frac{\Gamma_{us}}{\tanh(\sigma_{rs} c/2)} + \frac{\theta_{urs}(-1)^{s+1}}{\sinh(\sigma_{rs} c/2)} \right\} \right] \frac{\Lambda_{nr} \Lambda_{vr}}{J_r}$
S-A	$\frac{1}{2} \rho_o \sum_{m=1}^M \sum_{n=1}^N \sum_{u=1}^M \sum_{v=1}^N q_{uv} q_{mn} \sum_{r=1}^{\infty} \sum_{s=1}^{\infty} \left[\frac{\varphi_{ms}}{\alpha_{rs} E_s} \left\{ \frac{\chi_{urs}(-1)^{s+1}}{\sinh(\alpha_{rs} b/2)} + \frac{\varphi_{us}}{\tanh(\alpha_{rs} b/2)} \right\} \right. \\ \left. + \frac{\Gamma_{ms}}{\sigma_{rs} D_s} \left\{ \Gamma_{us} \tanh\left(\frac{\sigma_{rs} c}{2}\right) + \frac{\vartheta_{urs}(-1)^{s+1}}{\cosh(\sigma_{rs} c/2)} \right\} \right] \frac{\Lambda_{nr} \Lambda_{vr}}{J_r}$
A-S	$\frac{1}{2} \rho_o \sum_{m=1}^M \sum_{n=1}^N \sum_{u=1}^M \sum_{v=1}^N q_{uv} q_{mn} \sum_{r=1}^{\infty} \sum_{s=1}^{\infty} \left[\frac{\Omega_{ms}}{\alpha_{rs} C_s} \left\{ \frac{\kappa_{urs}(-1)^{s+1}}{\cosh(\alpha_{rs} b/2)} + \Omega_{us} \tanh\left(\frac{\alpha_{rs} b}{2}\right) \right\} \right. \\ \left. + \frac{\varepsilon_{ms}}{\sigma_{rs} \Delta_s} \left\{ \frac{\varepsilon_{us}}{\tanh(\sigma_{rs} c/2)} + \frac{\theta_{urs}(-1)^{s+1}}{\sinh(\sigma_{rs} c/2)} \right\} \right] \frac{\Lambda_{nr} \Lambda_{vr}}{J_r}$
A-A	$\frac{1}{2} \rho_o \sum_{m=1}^M \sum_{n=1}^N \sum_{u=1}^M \sum_{v=1}^N q_{uv} q_{mn} \sum_{r=1}^{\infty} \sum_{s=1}^{\infty} \frac{\varphi_{ms}}{\alpha_{rs} E_s} \left\{ \frac{\kappa_{urs}(-1)^{s+1}}{\cosh(\alpha_{rs} b/2)} + \varphi_{us} \tanh(\alpha_{rs} b/2) \right\} \\ + \frac{\varepsilon_{ms}}{\sigma_{rs} \Delta_s} \left\{ \varepsilon_{us} \tanh\left(\frac{\sigma_{rs} c}{2}\right) + \frac{\vartheta_{urs}(-1)^{s+1}}{\cosh(\sigma_{rs} c/2)} \right\} \right] \frac{\Lambda_{nr} \Lambda_{vr}}{J_r}$

where

$$\begin{aligned}
 \Gamma_{ms} &= \int_0^{b/2} H_m(x) \cos(\tau_s x) dx, & \chi_{urs} &= \int_0^{b/2} H_u(x) \cosh(\alpha_{rs} x) dx, \\
 \varepsilon_{ms} &= \int_0^{b/2} H_m(x) \sin(\tau_s x) dx, & \kappa_{urs} &= \int_0^{b/2} H_u(x) \sinh(\alpha_{rs} x) dx, \\
 \Omega_{ms} &= \int_0^{c/2} H_m(y + b/2) \cos(\beta_s y) dy, & \theta_{urs} &= \int_0^{c/2} H_u(y + b/2) \cosh(\sigma_{rs} y) dy, \\
 \varphi_{ms} &= \int_0^{c/2} H_m(y + b/2) \sin(\beta_s y) dy, & \vartheta_{urs} &= \int_0^{c/2} H_u(y + b/2) \sinh(\sigma_{rs} y) dy, \\
 D_s &= \int_0^{b/2} \cos^2(\tau_s x) dx, & C_s &= \int_0^{c/2} \cos^2(\beta_s y) dy, \\
 \Delta_s &= \int_0^{b/2} \sin^2(\tau_s x) dx, & E_s &= \int_0^{c/2} \sin^2(\beta_s y) dy, \\
 \Lambda_{nr} &= \int_0^d F_n(z) \cos(\lambda_r z) dz, & J_r &= \int_0^d \cos^2(\lambda_r z) dz.
 \end{aligned}$$